ORIGINAL RESEARCH ARTICLE

Effects of TiC Powder Characteristics and Sintering Temperature on the Microstructure and Mechanical Properties of TiC–20Mo–10Ni Cermets

XIAO-CHUN DENG, JIAN CUI, and GUO-HUA ZHANG

TiC–Mo–Ni cermets were prepared by vacuum sintering using Ni powder as well as the self-synthesized ultrafine TiC and Mo powders as raw materials. Ni used as sintering additive was added to activate the sintering process. The effects of TiC grain size and sintering temperature on mechanical properties and microstructure of TiC–Mo–Ni cermets were investigated. The results showed that Mo was dissolved into TiC phase to generate (Ti, Mo)C solid solution and form a typical core–rim structure. The grain size of cermets was greatly affected by the particle size of raw material TiC powders. In addition, the increases of oxygen content and grain size in TiC powder were detrimental to the densification of TiC–Mo–Ni cermets. By using the TiC powder obtained under the calcium treatment temperature of 1523 K, the TiC–20Mo–10Ni cermet sintered at 1773 K in vacuum had a high relative density (98.8 pct), uniform microstructure, fine grain size (1.49 μm) and excellent mechanical properties (with the Vickers hardness, fracture toughness, transverse rupture strength of 2081 HV_{30}, 11.43 $MPa{\cdot}m^{1/2}$ and 813 MPa, respectively). Moreover, the increase of TiC grain size led to the transition of fracture mechanism from intergranular fracture to transgranular fracture, which was favorable for the improvement of toughness.

https://doi.org/10.1007/s11661-023-07215-5

I. INTRODUCTION

TITANIUM carbide (TiC), due to its high melting point, superb wear resistance, satisfactory hardness and strength, is widely used in engineering materials such as drill tools, anti-abrasive coatings and mechanical parts.[1–4] However, the fracture toughness of TiC cermet is bad, which limits its application and development. The introduction of metal binders such as Fe, Co, Ni or Mo is a very effective way to improve the mechanical properties of TiC-based cermets.[5] Fe is one of the most commercial metallic binders due to its cheap price and excellent wettability with TiC,[2,6] while it has the limitation of poor anti-corrosion property.[7] Co exhibited several restrictions including its scarcity and enormous cost. Comparing with Co binder, Ni is more promising due to its stable market price and lower environmental toxicity.[8] However, the poor wettability between Ni and TiC (wetting angle is 30 deg in vacuum) leads to a low bonding strength and toughness.[9] In order to improve the wettability of Ni with TiC, Mo is added to enhance the driving force and densification.[10–12] Meanwhile, adding appropriate amount of Mo can inhibit the growth of grains, which is beneficial to improving the mechanical properties of cermets.[13] Consequently, the Mo binder played a significant role in refining grains and improving strength.

Zhou *et al.*[14] found that the Mo–Ni system had a low binary eutectic point at 1584 K which could effectively improve the sintering kinetics by forming the liquid phase locally. Ohser-Wiedemann *et al.*[15] prepared Mo–TiC composites with a relative density of 98 pct by spark plasma sintering, and found that adding TiC to molybdenum could significantly improve the hardness. Fu *et al.*[16] studied the effects of Mo and Ni contents on mechanical properties of TiC–Ni–Mo cermets. The results showed that adding appropriate amount (10 wt pct) of Mo could effectively reduce the grain size and improve the hardness and fracture toughness of TiC–Ni–Mo cermets. Acharya *et al.*[9] found that the addition of NiB improved the densification of TiC–Ni cermets. Moreover, when the content of NiB was 10 wt pct, the hardness of TiC–10Ni cermet reached the maximum value of 2759 HV_5. Zhang *et al.*[17] prepared TiCN–Mo coating with a good wear resistance by plasma spraying, which showed a lower wear rate and a higher friction coefficient than the coating without Mo.

XIAO-CHUN DENG, JIAN CUI, and GUO-HUA ZHANG are with the State Key Laboratory of Advanced Metallurgy, University of Science and Technology Beijing, Beijing 100083, P.R. China. Contact e-mail: ghzhang0914@ustb.edu.cn
Manuscript submitted May 14, 2023; accepted September 25, 2023.
Article published online October 4, 2023

At present, most of investigations used commercial large-sized TiC powder as raw material, and mainly studied the effects of Mo or Ni content on the properties and microstructure of cermets, while there are few studies about the influences of TiC characteristics including size and its oxygen content. The particle size of TiC is one of the key factors affecting the comprehensive properties of cermets. Consequently, it is essential to investigate the effect of this factor on the properties and microstructure of TiC–Mo–Ni cermets. In this study, TiC powder was prepared by the process of "carbothermal reduction + calcium treatment", TiC–20Mo–10Ni cermets were prepared by vacuum sintering using the self-synthesized ultrafine TiC with uniform particle size distribution as raw material. During the preparation of TiC powder, the calcium treatment temperature has great effects on its particle size and oxygen content. Therefore, it is necessary to investigate the effect of calcium treatment temperature on the microstructure and mechanical properties of TiC–20Mo–10Ni cermets, so as to provide some theoretical guidance for the preparation of TiC-based cermets with satisfactory comprehensive properties.

II. EXPERIMENTAL

A. *Materials and Preparation*

The basic parameters of the raw materials used in this study are listed in Table I. Ultrafine titanium carbide (TiC) powder was synthesized by carbothermal reduction method followed by calcium treatment.[18] First, TiO_2 was reduced by excessive carbon black (with the molar ratio of TiO_2 to C of 3.6) at 1723 K for 4 hours in vacuum, and then the reduced powders were reacted in calcium melt at different temperatures (1423 K, 1523 K and 1623 K) for 4 hours to remove the residual oxygen and free carbon. Finally, pure TiC powder was obtained after acidic leaching and denoted as TiC-*T* K, where *T* is the calcium treatment temperature. Mo powder was prepared by carbothermal reduction of MoO_3 at 873 K for 2 hours and then at 1323 K for 4 hours. Subsequently, high purity and ultrafine Mo powder was obtained by deep reduction of hydrogen at 1273 K for 4 hours.[19]

The sintering temperature and compositions of target cermets are listed in Table II. The TiC-*T* K, Mo and Ni powders were uniformly mixed by ball milling for 4 hours with 2 wt pct stearic acid. The milling balls and jars were made of stainless steel. The ball-to-powder weight ratio and rotational speed were 5:1 and 200 rpm, respectively. The mixture was pressed into green compact with a size of 16 mm × 12 mm under a uni-axial pressure of 100 MPa. The green compacts were firstly heated to degreasing temperature (673 K) with a heating rate of 2 $K \cdot min^{-1}$ and maintained for 2 hours, and then heated to sintering temperature (1773 K, 1748 K and 1723 K) with a heating rate of 5 $K \cdot min^{-1}$ and maintained for 4 hours under vacuum conditions (0.2 Pa) to prepare TiC–20Mo–10Ni cermets.

B. *Characterizations of Composition and Microstructure*

The phase composition and morphology of the samples were characterized by X-ray diffraction (XRD, TTR III, Rigaku Corporation, Japan; 1.5406 Å [Cu-Kα]) and scanning electron microscope (SEM, ZEISS SUPRA 55, Oberkochen, Germany), respectively. Energy dispersive spectrometer (EDS) was used to characterize the elemental distribution of the samples. The carbon and oxygen contents were detected *via* infrared carbon–sulfur analyzer (EMIA-920V2, HORIBA, Japan) and oxygen–nitrogen–hydrogen analyzer (EMGA-830AC, HORIBA, Japan). The average grain size was obtained by randomly measuring 300 grains using linear intercept method.

C. *Properties Characterizations*

The as-sintered samples were ground and polished to near-mirror finish before properties characterizations. The Vickers hardness (HV) was measured by a Vickers indenter (VTD510P, Beijing Wowei Science and

Table I. Basic Parameters of the Raw Materials

Raw Materials	Purity (Pct)	Particle Size	Manufacturers
TiO_2	99.8	25 nm	Shanghai Xiang Tian Nanomaterials Co. Ltd.
MoO_3	99.9	70 μm	Jinduicheng Molybdenum Co., Ltd.
Ni Powder	98.0	~ 10 μm	Shanghai Macklin Biochemical Co., Ltd.
Carbon Black	98.5	< 100 nm	Mitsubishi Chemical Corporation

Table II. Sintering Temperature and Compositions of Target Cermets

No.	Sintering Temperature (K)	TiC Powders	TiC (Wt pct)	Mo (Wt pct)	Ni (Wt pct)
A	1773	TiC-1423 K	70	20	10
B	1773	TiC-1523 K	70	20	10
C	1773	TiC-1623 K	70	20	10
D	1748	TiC-1523 K	70	20	10
E	1748	TiC-1623 K	70	20	10
F	1723	TiC-1523 K	70	20	10
G	1723	TiC-1623 K	70	20	10

Technology Co., Ltd.) with a load of 30 kg. The transverse rupture strength (TRS) was measured by the three-point bending method (CDW-5, Changchun City Chaoyang Test Instrument Co., Ltd.) with a loading rate of 0.5 mm/min. The three-point bending strength was calculated by Eq. [1]:[20]

$$R = 3FL/2bh^2 \quad [1]$$

where R is the TRS (MPa); F is the load (kg); L is the fixture span (mm); b and h are the width and thickness of specimen (mm), respectively. The fracture toughness (K_{IC}) was calculated by Palmqvist indentation method[21] and the calculation method was shown in Eq. [2]:

$$K_{IC} = 0.0028\sqrt{HV_{30} \cdot P/\sum l} \quad [2]$$

where HV_{30} is the Vickers hardness (N/mm^2); P is the load (N); $\sum l$ is the sum of the crack length (mm). The relative density was measured through Archimedes method.

III. RESULTS AND DISCUSSION

A. *Phase Composition and Microstructure of Powders*

The XRD patterns and SEM images of the synthesized raw materials are shown in Figure 1. It can be seen from Figure 1(a) that pure TiC and Mo powders are prepared. The SEM images of TiC powders obtained at

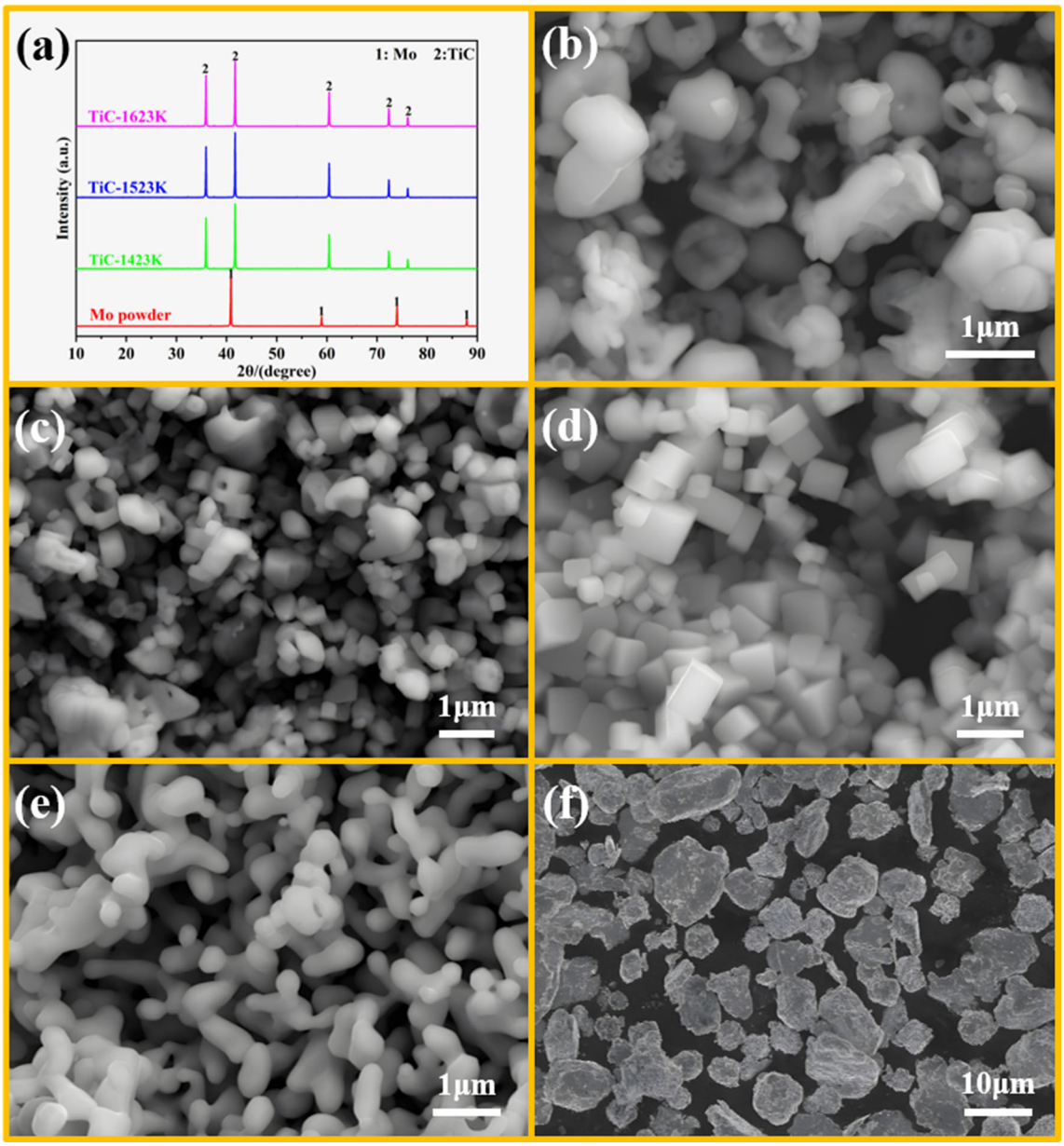

Fig. 1—(*a*) XRD pattern of TiC and Mo powders; SEM images of (*b*) TiC-1423 K, (*c*) TiC-1523 K, (*d*) TiC-1623 K, (*e*) Mo powder, (*f*) Ni powder.

Table III. Relevant Parameters of TiC, Mo and Ni Powders

Sample	Carbon Contents (Wt Pct)	Oxygen Contents (Wt Pct)	Grain Size (μm)
TiC-1423 K	19.44	0.63	0.41
TiC-1523 K	19.72	0.26	0.46
TiC-1623 K	19.81	0.22	0.56
Mo Powder	0.01	0.24	0.32
Ni Powder	0.06	0.15	~ 10

different calcium treatment temperatures are shown in Figures 1(b) through (d), and the relevant parameters are present in Table III. From Figures 1(b) through (d), with the calcium treatment temperature increases, the grains gradually change to the stable cube morphology. The average particle sizes of TiC prepared at different calcium treatment temperatures (1423 K, 1523 K and 1623 K) are 0.41, 0.46 and 0.56 μm, respectively. Meanwhile, the corresponding oxygen contents of TiC powders are 0.63, 0.26 and 0.22 wt pct, respectively, indicating that the increase of calcium treatment temperature is beneficial to the removal of residual oxygen. The average grain size of Mo powder prepared after carbothermal reduction and hydrogen deep reduction is about 0.32 μm, as shown in Figure 1(e). In Figure 1(f), Ni is block-shaped particle with average particle size of about 10 μm. In addition, the carbon and oxygen contents of Mo and Ni powders are low.

B. *Relative Density*

The relative densities of all as-sintered cermets are given in Figure 2. From Figure 2, the relative densities of sample A, sample B and sample C are 94.4, 98.8 and 96.9 pct, respectively. The relative density increases first and then decreases with the increase of TiC grain size. This may be due to the fact that excessive oxygen content and large TiC grain size lead to a weaker sintering activity, and therefore, sample B has the highest relative density among samples A to C. Kang *et al.*[22] found that severe surface oxidation of raw materials would hinder the densification of cermets. Therefore, only TiC-1523 K and TiC-1623 K powders were selected as raw materials to study the effect of sintering temperature on the microstructure and mechanical properties of cermets. For a given calcium treatment temperature, the relative density of cermet increases with the increase of sintering temperature. This may be because increasing temperature can accelerate grain boundary diffusion and thus improve the densification of cermets. In addition, the densification depends mainly on the amount of liquid phase formed.[9] As the sintering temperature increases, the amount of liquid phase in the system increases, resulting in more pores being filled and larger densification degree.

C. *Phase Composition and Microstructure of all As-Sintered Samples*

The XRD patterns of all as-sintered samples are shown in Figure 3. There are only Ni and TiC phases in all samples, and no diffraction peak of Mo is observed, probably due to that Mo can react with TiC and Ni. The local magnified XRD patterns corresponding to peaks a, b, and c in Figure 3(a) of samples A, B, and C are shown in Figure 4(a). Obviously, compared with the standard peaks of TiC, the TiC peaks of samples A, B and C shift to a higher angle (low interplanar spacing).[10] Fu *et al.*[16] found that with the increase in Mo content, Ni peaks shifted to a lower angle, while TiC peaks slightly shifted to a higher angle. This is mainly because of the dissolution of Mo into TiC to form (Ti, Mo)C solid solution during sintering, as well as the formation of Ni–Mo–Ti alloy. The similar results was also found by Jõeleht *et al.*[23] In addition, from Figures 4(b) and (c), TiC peaks slightly shift to a higher angle and interplanar spacing reduces with increasing calcium treatment temperature. This may be attributed to that with the increase of calcium treatment temperature, calcium metal (as a deoxidizer) reacts more thoroughly with oxygen, leading to a decrease in residual oxygen of TiC. The decrease of oxygen content in TiC powder can accelerate the diffusion of Mo into TiC to form (Ti, Mo)C solid solution. Since the atomic radius of Ti (0.14318 nm) is larger than that of Mo (0.13626 nm), the formation of (Ti, Mo)C reduces the interplanar spacing of TiC.

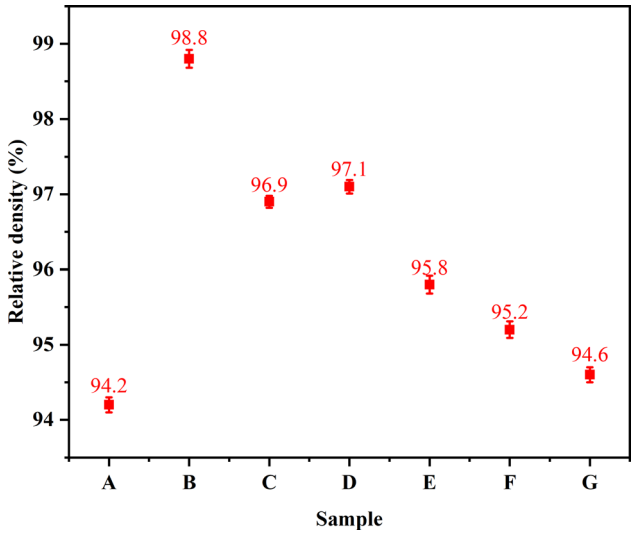

Fig. 2—Relative densities of all as-sintered samples.

Figure 5 exhibits the SEM images and grain size distributions of TiC–Mo–Ni cermets sintered at 1773 K with different TiC raw materials. Compared with samples A and C, most of the pores in sample B are eliminated, but some micropores still exist. The porosity of sintered samples is related to the oxygen content of raw TiC powder. As the oxygen content of TiC-1423 K powder is higher than that of TiC-1523 K and TiC-1623 K powders, the relative density of the corresponding sintered sample is lower. This is because oxygen may exist in the form of TiC_xO_{1-x} in TiC powder. The wettability of Ni and TiC_xO_{1-x} is poorer that of TiC, and thus, the cermet remains porous during vacuum sintering.[11]

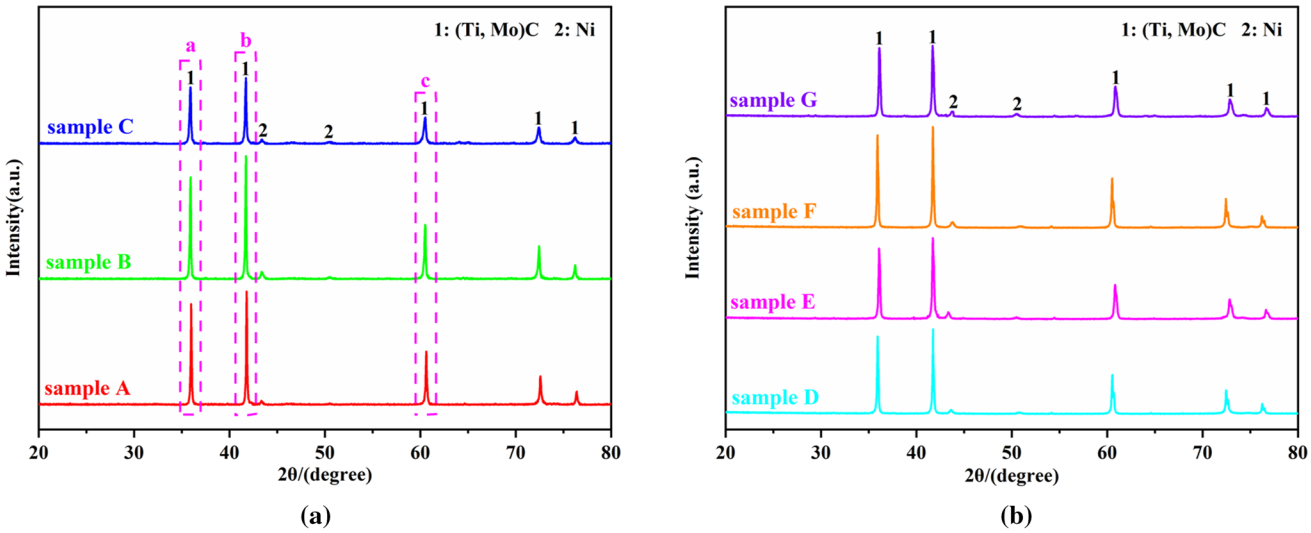

Fig. 3—XRD patterns of all as-sintered samples at different sintering temperatures (*a*) 1773 K, (*b*) 1748 K and 1723 K.

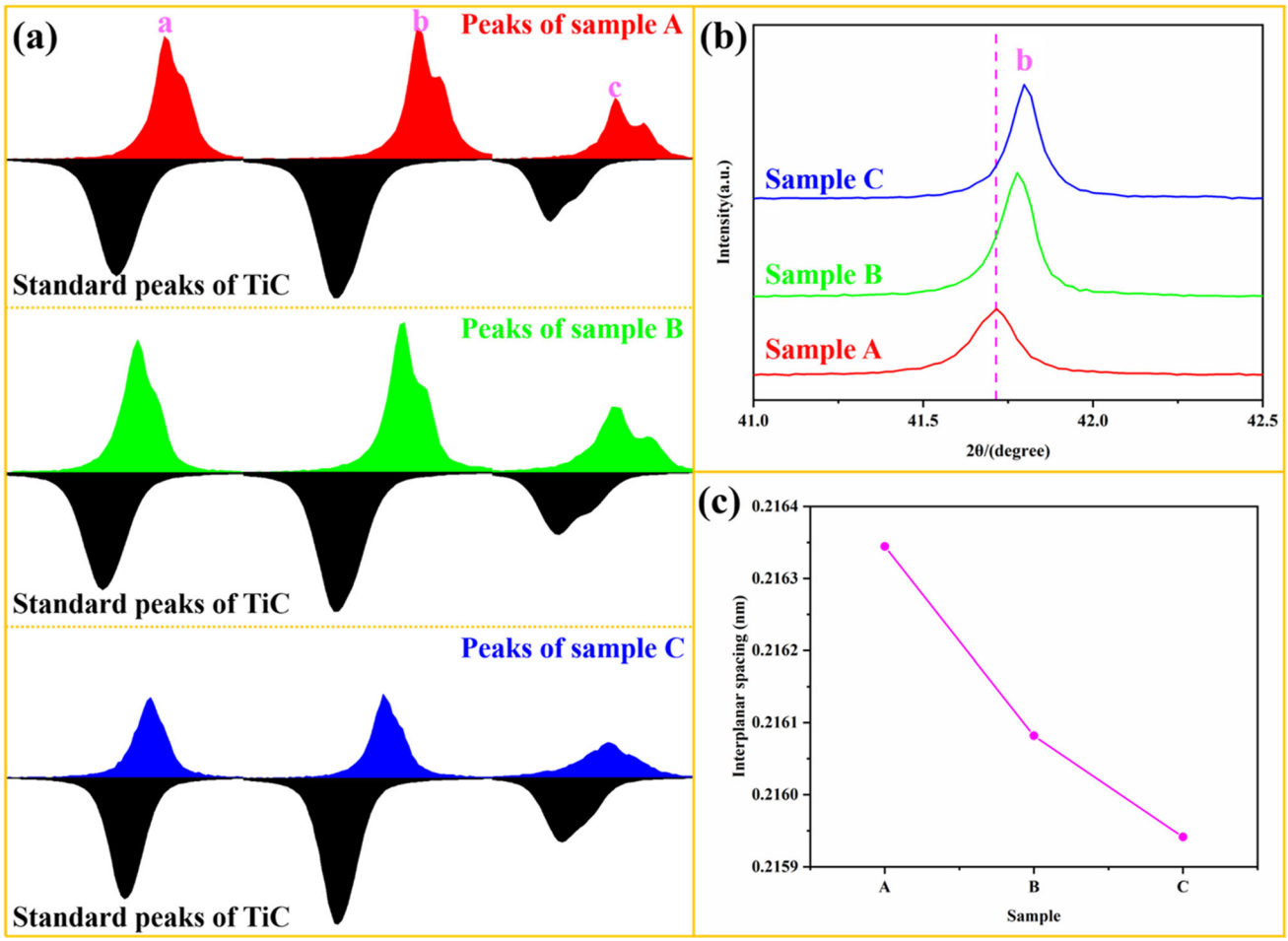

Fig. 4—(*a*) Local magnified XRD patterns (corresponding to Fig. 3(a)) of peaks a, b and c, (*b*) local magnified XRD patterns of peak b, (*c*) interplanar spacing corresponding to peak b of TiC phase.

The average grain sizes of sample A, B and C are 1.01 ± 0.35, 1.49 ± 0.49 and 1.54 ± 0.57 μm, respectively, which has a positive correlation with the particle size of raw TiC powders. Fu *et al.*[16] found that the utilization of ultra-fine TiC powders significantly decreased the grain size and changed the grain

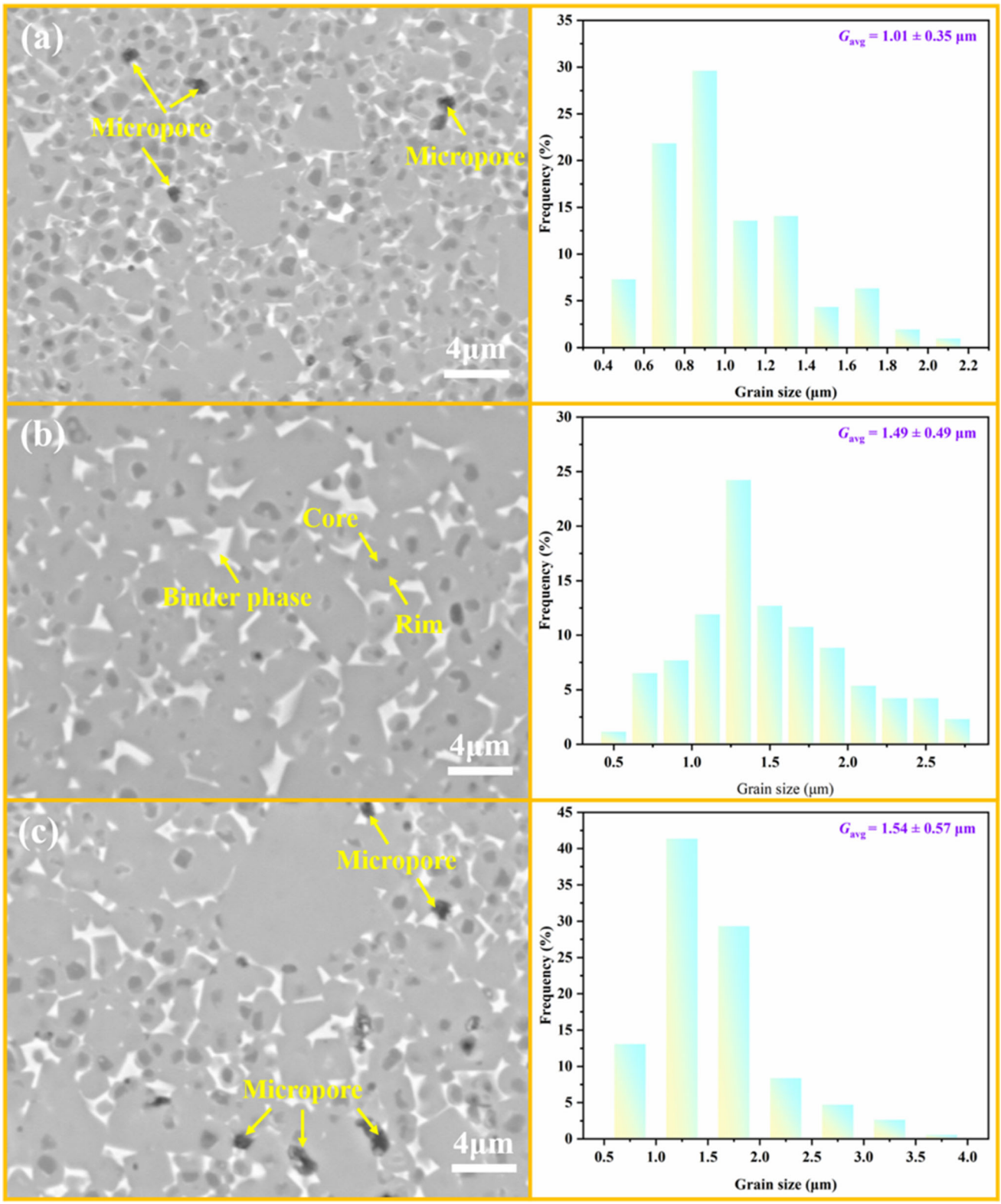

Fig. 5—SEM images and grain size distributions of TiC-Mo-Ni cermets sintered at 1773 K (*a*) sample A, (*b*) sample B, (*c*) sample C.

morphology. There are abnormally grown grains in samples A and C, while the grain size distribution of sample B is uniform. After sintering, all samples form a typical core–rim structure. According to the SEM image (Figure 5(b)), there are three different phases in the sample: dark core, gray rim and light gray phases. Combined with the element distribution in Figure 6, it can be concluded that the dark core, gray rim and light

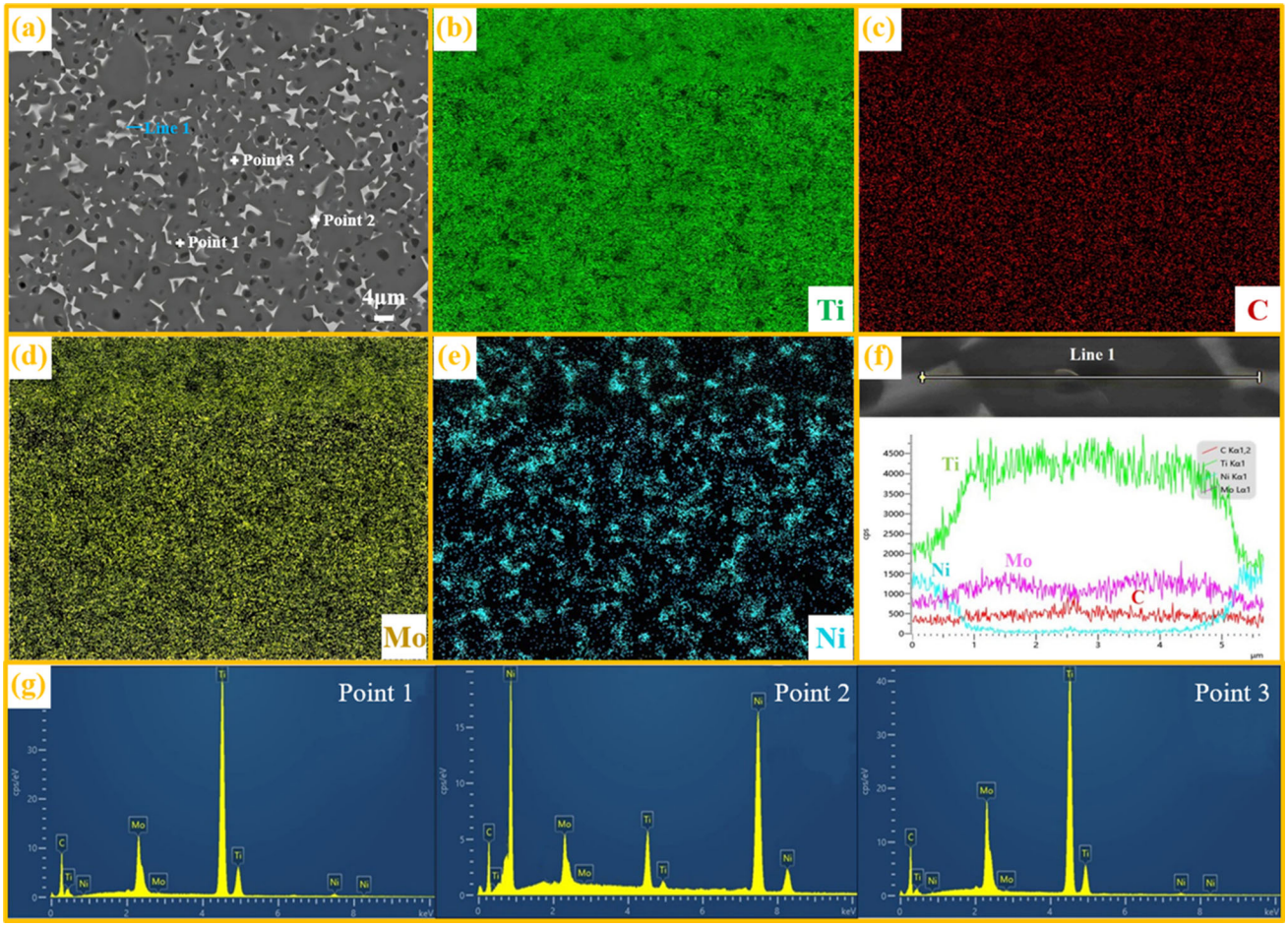

Fig. 6—(*a*) SEM image of sample B and its corresponding element distributions (*b*) Ti element, (*c*) C element, (*d*) Mo element, (*e*) Ni element, (*f*) EDS result of line 1, (*g*) EDS results of points 1, 2 and 3.

gray phases are the undissolved TiC phase, the complex solid solution phase of (Ti, Mo)C, and the Ni binder phase, respectively, which is consistent with the XRD results. In addition, the content of Mo in the gray phase is significantly higher than that in the dark core. Ni forms Ni–Mo–Ti alloy with small amounts of Mo and Ti, which also confirms the shift of Ni peaks due to the formation of Ni–Mo–Ti alloy in XRD analysis.[24]

The concentration distributions of Ti, Mo, Ni and C were studied by line scanning method, and the results are shown in Figure 6(f). The concentration of Ni decreases from the core to the binder phase, while the concentration of Ti increases. Compared with the binder phase and dark core, the content of Mo in the gray phase is relatively higher. This also confirms the formation of the core–rim structure with Ni as the binder phase, TiC as the black core, and (Ti, Mo)C as the gray rim. The gray rim phase is the complex solid solution of (Ti, Mo)C formed by the diffusion of Mo into TiC. The formation of the core–rim structure is resulted from the co-existence of metallic and ceramic phases to create two interlocking skeletons.[25]

Figure 7 shows the SEM images and grain size distributions of TiC–Mo–Ni cermets sintered at 1748 K and 1723 K with different TiC raw materials. All the samples show a typical core–rim structure, and the number of pores reduces as the sintering temperature increases, which is consistent with the variation of relative density in Figure 2. This also indicates that sintering temperature has an important influence on relative density. The grain sizes of sample D, sample E, sample F, sample G are 1.25 ± 0.46, 1.50 ± 0.42, 1.11 ± 0.32 and 1.14 ± 0.38 μm, respectively. With the increases of sintering temperature and calcium treatment temperature, the grain size of TiC increases. The TiC grains in TiC-based cermets are grown mainly through dissolution–precipitation rather than coalescence.[26] The grain boundary migration of TiC grains increases with the increase of sintering temperature, and thus, TiC grains become larger if the sintering temperature becomes higher. Matsubara *et al.*[27] found that the growth rate constant of TiC is related to sintering temperature. With the increase of sintering temperature, the diffusion kinetics and the dissolution–precipitation rates accelerate, thus promoting the growth of grains. Meanwhile, the increase in volume fraction of liquid phase can also increases the growth rate of grains.[28]

From Figures 7(a) and (b), it is obvious that the black core of sample E is larger than that of sample D. This is mainly because the grain size of TiC in sample E is

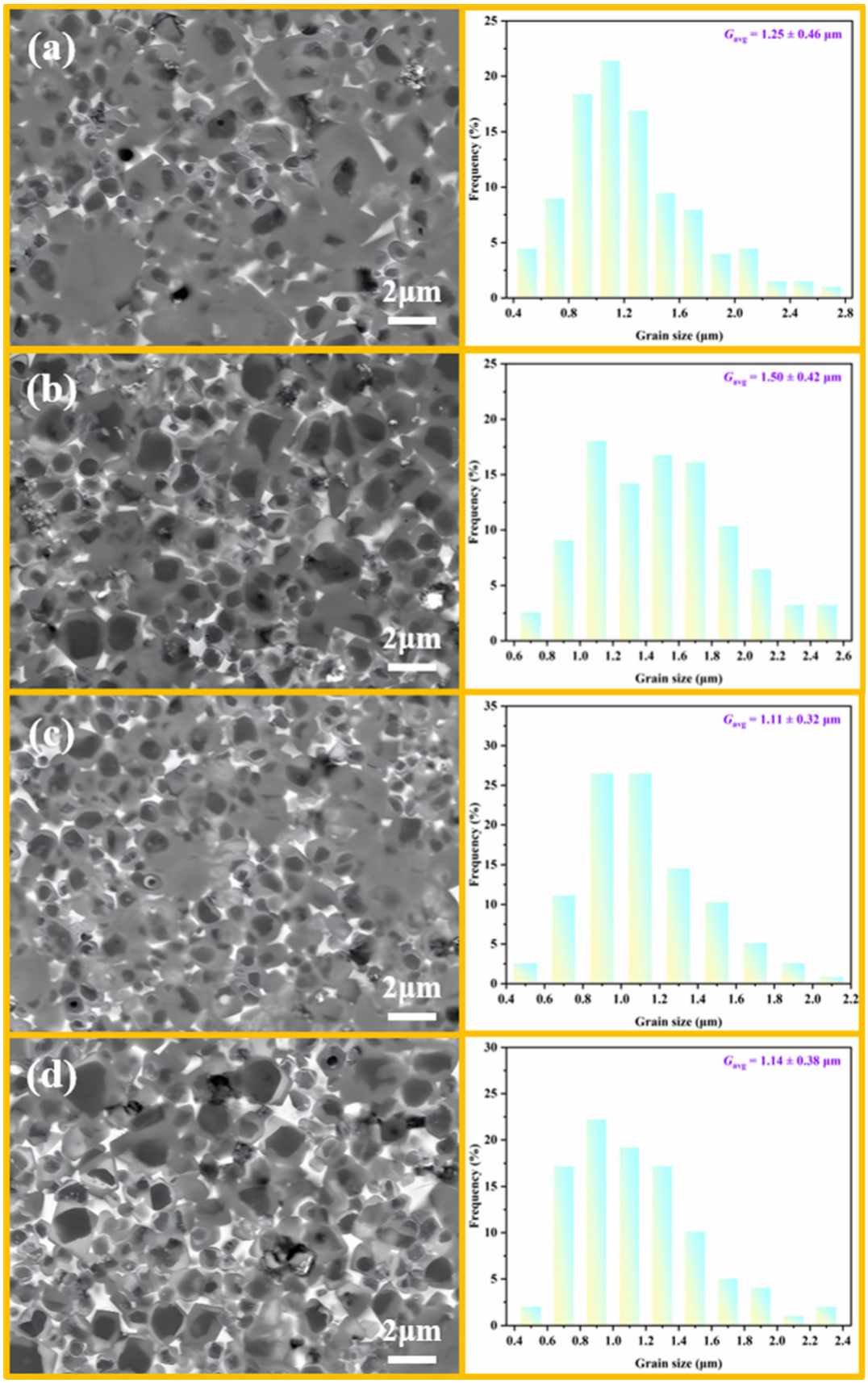

Fig. 7—SEM images and grain size distributions of the as-sintered (*a*) sample D, (*b*) sample E, (*c*) sample F, (*d*) sample G.

larger than that of sample D. When sintering temperature is the same, the diffusion rate of Mo atom is the same. The small-sized TiC grains may have a lower thermodynamic stability and shorter diffusion distance for Mo atoms than coarsened TiC grains.[10] Thus, Mo atoms are readily to diffuse into the lattice of TiC to form the (Ti, Mo)C solid solutions.

D. *Mechanical Properties*

Figure 8 shows the hardness, fracture toughness and transverse rupture strength of all as-sintered samples. For a given sintering temperature, with the increase of calcium treatment temperature, the hardness of samples A to C increases first and then decreases. As we all know, the hardness of cermets is mainly related to grain size and relative density.[29] According to the Hall–Petch relationship, finer grains provide a higher grain boundary strengthen, which results in a higher hardness.[16,30] Compared with sample B, sample A has a smaller grain size but a lower relative density. For sample C, larger grain size and smaller relative density are not conducive to improving the hardness of cermets. In summary, sample B with uniform microstructure has the maximum hardness value of 2081 HV_{30} in samples A–C. In addition, for samples A–C, the interplanar spacing of TiC phase increases with the decrease in particle size of raw TiC powder, indicating the formation of more (Ti, Mo)C solid solutions.[16] In general, due to the presence of lattice distortion in the solid solution, there is a high hardness of the solid solution.[31] By using the same raw TiC powder, the hardness of cermet shows a decreasing trend with the decrease of sintering temperature, owing to the decreases in relative density. Though the lower sintering temperature leads to the smaller grain size of TiC, the decrease in relative density plays a dominant role, thus resulting in a decrease in the hardness of cermets. Wang *et al.* found that the hardness of cermets increased with the increase of relative density.[32] Moreover, with the increase of sintering temperature, the diffusion rate of Mo atom is accelerated, and the dissolution of Mo into TiC phase is promoted to form more (Ti, Mo) C solid solutions, which is conducive to improving the hardness of cermets.

Fracture toughness and transverse rupture strength are also important mechanical properties indicators to evaluate cermets. The grain size and relative density of the cermets are the key factors in fracture toughness and transverse fracture strength. It is not difficult to find that the fracture toughness and transverse rupture strength of the samples follow the same trend as the hardness. For samples A, B and C, the K_{IC} and TRS of sample B reach the peak values of 11.43 MPa·$m^{1/2}$ and 813 MPa, respectively. Compared with sample A (1.01 μm), the grain size of sample B (1.49 μm) is larger, which is favorable to improve the fracture toughness. This is because the small-sized grains cannot accommodate more mobile dislocations, thus leading to a decrease in fracture toughness.[33] Meanwhile, the large-sized grains can inhibit crack propagation and have the characteristics of high toughness.[31] In addition, the grain size of sample C (1.54 μm) is slightly larger than that of sample B (1.49 μm), while the relative density of sample C (96.9 pct) is much smaller than that of sample B (98.8 pct). A high relative density can also increase the fracture toughness, since the micropores in the sample act as crack initiation and crack propagation sites, which will lead to a decline of fracture toughness.[34] Meanwhile, the increase in the number of pores will worsen the interfacial adhesion and result in brittle fracture. For the

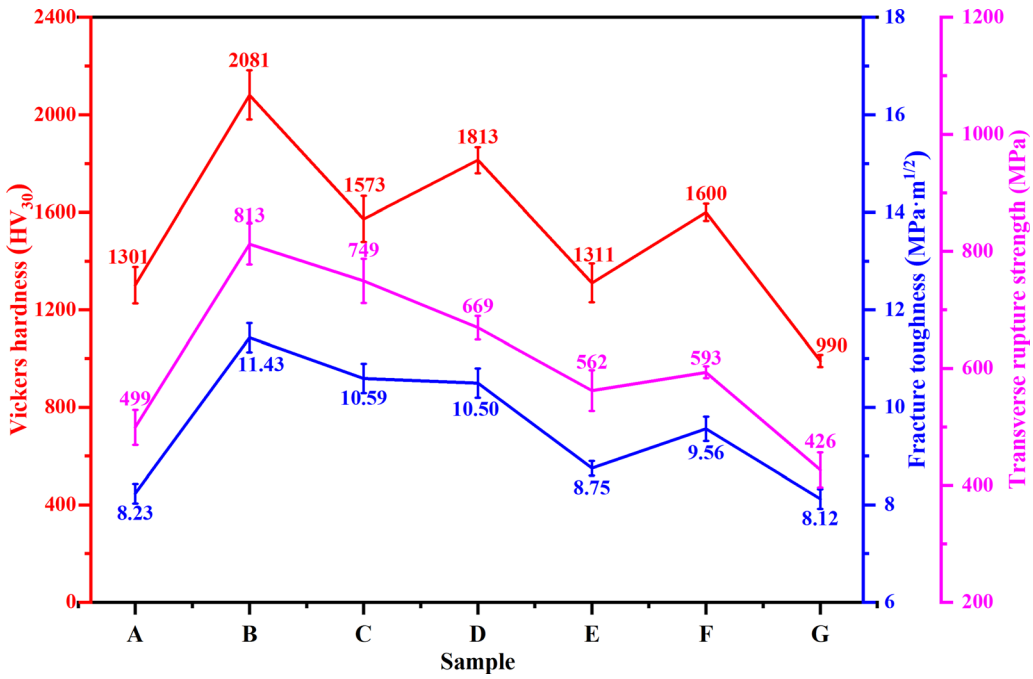

Fig. 8—HV_{30}, K_{IC} and TRS of all cermets.

same raw TiC powder used, the grain size and relative density of the samples decreased as the sintering temperature decreased. Because small-sized grains cannot contain too much mobile dislocations, there will be deterioration of the fracture toughness.[35]

Figure 9 shows a comparison of mechanical properties between TiC-based cermets reported in literatures[9,10,16,22,29,36] and the TiC–20Mo–10Ni cermet prepared in this work. The currently prepared TiC–20Mo–10Ni cermet has excellent comprehensive mechanical properties. This may be due to the more homogeneous microstructure and finer grain size in the cermets resulting from the self-synthesized high purity ultra-fine Mo and TiC powders. It has been reported that the use of ultra-fine TiC powder is conducive to improving the driving force of sintering, resulting in high relative density, fine microstructure and excellent mechanical properties.[5] In addition, the addition of metal Mo not only improves the wettability of TiC and Ni, but also strengthens the TiC/TiC grain boundary and TiC/Ni phase boundary.[10,12,13,37] This is beneficial to improving the mechanical properties of cermets. Meanwhile, Mo could react with TiC to form (Ti, Mo)C solid solution. Generally speaking, due to the existence of a large number of lattice distortions in the solid solutions, the hardness of the solid solutions is relatively high, while the toughness will be low.[31]

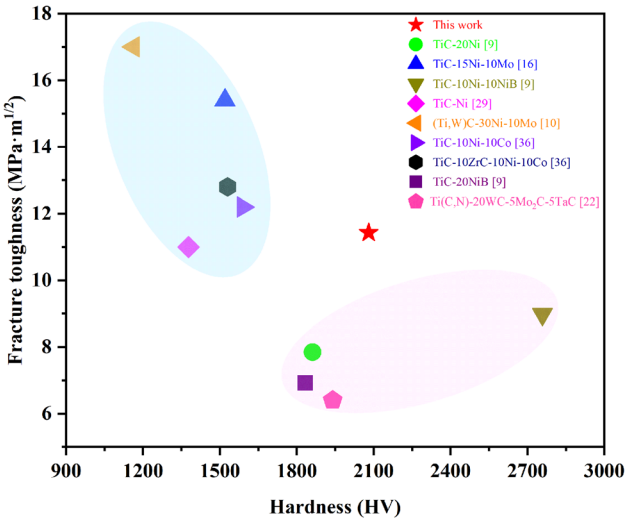

Fig. 9—Comparison of mechanical properties with other reported TiC-based cermets.

E. *Fracture Mechanism*

Crack propagation images originating from the corners of the Vickers hardness indentations of the TiC–Mo–Ni cermets are shown in Figure 10. From Figures 10(a) through (c), there are two fracture modes including intergranular fracture and transgranular fracture in TiC–Mo–Ni cermets. With the increase in particle size of raw TiC powder, the main crack propagation mode of sintered cermet changes from intergranular fracture to transgranular fracture. In other words, transgranular fracture is more likely to occur in cermet with coarse carbide grains, while intergranular fracture is prone to occur in cermet with small-sized carbide grains. During crack propagation, coarse TiC grains will hinder crack growth, and transgranular fracture can consume more energy, which are beneficial to improve fracture toughness.[38–40] In addition, for samples A–C, with the decrease in particle size of raw TiC powder, more (Ti, Mo)C solid solutions are formed. In general, the solid solution is more brittle than TiC, so the formation of (Ti, Mo)C solid solution has an adverse effect on the fracture toughness of cermet. However, Mo reacts with the ceramic phase TiC to generate (Ti, Mo)C solid solution, which improves the wettability between the ceramic phase and the binder phase, thus improving the toughness. Moreover, with the decrease of calcium treatment temperature, the oxygen content of TiC powder increases, which is not conducive to the densification of cermets. Considering the influence of the

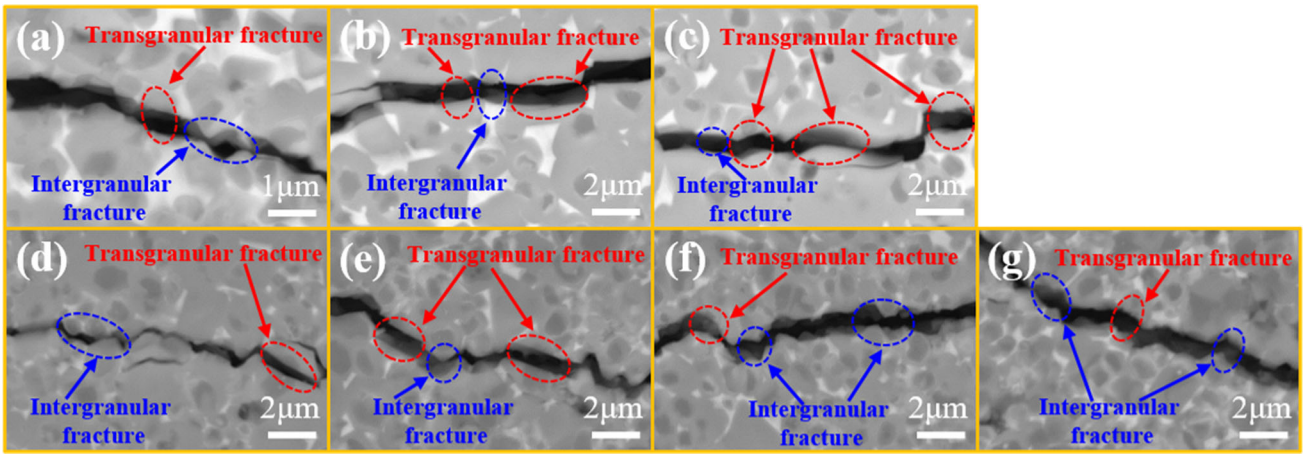

Fig. 10—Crack propagation images of (*a*) sample A, (*b*) sample B, (*c*) sample C, (*d*) sample D, (*e*) sample E, (*f*) sample F, (*g*) sample G.

above factors, sample B has the best toughness among samples A–C. In Figures 10(b) and (c), there are crack bridges, which is the main toughening mechanism in samples B and C. From Figures 10(d) through (g), compared with samples B and C, the carbide grain sizes of samples D–G are reduced and the intergranular fracture becomes the main crack propagation mode, which is bad for toughness. This is mainly due to that the small-sized grains cannot accommodate more mobile dislocations, thus resulting in a decrease in fracture toughness.

IV. CONCLUSION

The high performance TiC–20Mo–10Ni cermets were effectively prepared by vacuum sintering, using the raw materials of Ni powder as well as self-synthesized ultrafine Mo and TiC powders. The microstructure and mechanical properties of sintered samples were studied and the following conclusions were drawn:

(1) With the increase of calcium temperature during the preparation of TiC powder, the particle size of TiC increased, while the oxygen content decreased. Large grain size and high oxygen content were detrimental to the densification of cermets.
(2) The TiC–20Mo–10Ni cermet obtained by vacuum sintering of TiC-1523 K powder at 1773 K had the best comprehensive mechanical properties, with the hardness of 2081 HV_{30}, transverse rupture strength of 813 MPa, and fracture toughness of 11.43 $MPa{\cdot}m^{1/2}$.
(3) The sintered samples had a typical core–rim structure, in which the dark core was the undissolved TiC phase, and the gray rim was the (Ti, Mo)C solid solution phase.
(4) With the increase of grain size, transgranular fracture became the dominant fracture mode, which improved the fracture toughness of the cermets.

ACKNOWLEDGMENTS

The authors gratefully acknowledge financial support from the State Key Laboratory of Advanced Metallurgy, University of Science and Technology Beijing, China.

CONFLICT OF INTEREST

We declare that we have no financial and personal relationships with other people or organizations that can inappropriately influence our work, there is no professional or other personal interest of any nature or kind in any product, service and/or company that could be construed as influencing the position presented in, or the review of, the manuscript entitled.

REFERENCES

1. A. Jam, L. Nikzad, and M. Razavi: *Ceram. Int*., 2016, vol. 43, pp. 2448–55.
2. A. Rajabi, M.J. Ghazali, J. Syarif, and A.R. Daud: *Chem. Eng. J*., 2014, vol. 255, pp. 445–52.
3. S.A. Jung, H. Kwon, C.Y. Suh, J.M. Oh, and W. Kim: *Ceram. Int*., 2015, vol. 41, pp. 14326–31.
4. H. Kwon, S.A. Jung, C.Y. Suh, K.M. Roh, W. Kim, and J. Kim: *Ceram. Int*., 2015, vol. 41, pp. 4656–61.
5. Q.M. Zhuang, N. Lin, Y.H. He, and X.Y. Kang: *Ceram. Int*., 2017, vol. 43, pp. 15992–98.
6. S. Goto, Y. Nishijima, and H. Yoshinaga: *Trans. Jpn. Inst. Met*., 1987, vol. 28, pp. 550–57.
7. N. Liu, Y. Xu, Z. Li, M. Chen, G. Li, and L. Zhang: *Ceram. Int*., 2003, vol. 29, pp. 919–25.
8. S.H. Chang and P.Y. Chang: *Mater. Sci. Eng. A*, 2014, vol. 606, pp. 150–56.
9. S. Acharya, M. Debata, T.S. Acharya, P.P. Acharya, and S.K. Singh: *J. Alloys Compd*., 2016, vol. 685, pp. 905–12.
10. G.P. Zhang, W.H. Xiong, Q.Q. Yang, Z.H. Yao, S. Chen, and X. Chen: *Int. J. Refract. Met. Hard Mater*., 2014, vol. 43, pp. 77–82.
11. M. Jõeleht, J. Pirso, K. Juhani, M. Viljus, and R. Traksmaa: *J. Alloys Compd*., 2015, vol. 636, pp. 381–86.
12. Q.Z. Xu, X. Ai, J. Zhao, F. Gong, J.M. Pang, and Y.T. Wang: *J. Alloys Compd*., 2015, vol. 644, pp. 663–72.
13. B.L. Liu, S.G. Huang, J.V. Humbeeck, and J. Vleugels: *J. Alloys Compd*., 2017, vol. 712, pp. 579–87.
14. S.H. Zhou, Y. Wang, C. Jiang, J.Z. Zhu, L.Q. Chen, and Z.K. Liu: *Sci. Eng. A*, 2005, vol. 397, pp. 288–96.
15. R. Ohser-Wiedemann, C. Weck, U. Martin, A. Müller, and H.J. Seifert: *Int. J. Refract. Met. Hard Mater*., 2012, vol. 32, pp. 1–6.
16. Z.Z. Fu, J.H. Kong, S.R. Gajjala, and R. Koc: *J. Alloys Compd*., 2018, vol. 751, pp. 316–23.
17. F. Zhang, C. Li, S. Yan, J. He, B. Liu, and F. Yin: *Appl. Surf. Sci*., 2019, vol. 464, pp. 88–98.
18. K.H. Wu, Y. Jiang, S. Jiao, K.C. Chou, and G.H. Zhang: *J. Mater. Res. Technol*., 2020, vol. 9, pp. 11778–90.
19. G.D. Sun, G.H. Zhang, X.P. Ji, J.K. Liu, H. Zhang, and K.C. Chou: *Int. J. Refract. Met. Hard Mater*., 2019, vol. 80, pp. 11–22.
20. Y. Gao, M.Y. Yan, B.H. Luo, S. Ouyang, W. Chen, Z.H. Bai, H.B. Jing, and W.W. Zhang: *Mater. Sci. Eng. A*, 2017, vol. 687, pp. 259–68.
21. X.C. Deng, H. Zhang, and G.H. Zhang: *Int. J. Refract. Met. Hard Mater*., 2022, vol. 108, 105938.
22. X.Y. Kang, Y.H. He, N. Lin, M.M. Zhang, Y. Yan, and J.H. Huang: *J. Alloys Compd*., 2020, vol. 843, 155941.
23. M. Jõeleht, J. Pirso, K. Juhani, M. Viljus, and R. Traksmaa: *Int. J. Refract. Met. Hard Mater*., 2014, vol. 43, pp. 284–90.
24. W. Wan, J. Wang, M. Liang, K. Fan, Z. Wang, and Y. Li: *Ceram. Int*., 2022, vol. 48, pp. 32399–408.
25. M. Viljus, J. Pirso, K. Juhani, and S. Letunovitš: *Mater. Sci*., 2012, vol. 18, pp. 62–65.
26. H. Kwon and C.Y. Suh: *J. Alloys Compd*., 2020, vol. 834, 155000.
27. S. Shin, H. Matsubara, and T. Sakuma: *Solid State Phenom*., 1992, vol. 25–26, pp. 551–58.
28. M. Pellan, S. Lay, J.M. Missiaen, S. Norgren, J. Angseryd, E. Coronel, and T. Persson: *J. Am. Ceram. Soc*., 2015, vol. 98, pp. 3596–3601.
29. C. Zhang, Y. Du, S.Z. Zhou, Y.B. Peng, and J. Wang: *Ceram. Int*., 2016, vol. 42, pp. 19289–95.
30. Z. Fu and R. Koc: *Mater. Sci. Eng. A*, 2017, vol. 702, pp. 184–88.
31. X.C. Deng, X. Lan, Y.L. Wang, and G.H. Zhang: *Int. J. Refract. Met. Hard Mater*., 2023, vol. 111, 106103.
32. T.L. Wang, X.R. Zhao, Y.H. Fang, and M.X. Zhang: *Ceram. Int*., 2022, vol. 48, pp. 37275–86.
33. W.Z. Wang, Z.G. Chen, and S.S. Feng: *Materials*, 2019, vol. 12, p. 2901.
34. Z. Huang, X.R. Ren, M.X. Liu, C. Xu, X.H. Zhang, S.D. Guo, and H. Chen: *Int. J. Refract. Met. Hard Mater*., 2017, vol. 62, pp. 155–60.
35. X.W. Liu, X.Y. Song, H.B. Wang, X.M. Liu, X.L. Wang, and G.S. Guo: *J. Appl. Crystallogr*., 2015, vol. 48, pp. 1254–63.
36. X.B. Zhang and N. Liu: *Mater. Sci. Eng. A*, 2013, vol. 561, pp. 270–76.

37. Q.Z. Xu, J. Zhao, X. Ai, W.Z. Qin, D.W. Wang, and W.M. Huang: *J. Alloys Compd.*, 2015, vol. 649, pp. 885–90.
38. W. Dong, S. Zhu, H. Qu, and X. Liu: *Adv. Appl. Ceram.*, 2003, vol. 86, pp. 152–54.
39. L. Llanes, Y. Torres, and M. Anglada: *Acta Mater.*, 2002, vol. 50, pp. 2381–93.
40. W. Su, J. Zou, and L. Sun: *Int. J. Refract. Met. Hard Mater.*, 2020, vol. 92, 105337.